



## Modeling Real-Time Wellbore Stability within the Theory of Poromechanics

Younane Abousleiman, Rajesh Nair and Vinh Nguyen

Poromechanics Institute, PMI, the University of Oklahoma, USA.

Copyright 2003 AADE Technical Conference

This paper was prepared for presentation at the AADE 2003 National Technology Conference "Practical Solutions for Drilling Challenges", held at the Radisson Astrodome Houston, Texas, April 1 - 3, 2003 in Houston, Texas. This conference was hosted by the Houston Chapter of the American Association of Drilling Engineers. The information presented in this paper does not reflect any position, claim or endorsement made or implied by the American Association of Drilling Engineers, their officers or members. Questions concerning the content of this paper should be directed to the individuals listed as author/s of this work.

### Abstract

Real-Time wellbore stability mud weight estimates, while drilling, are becoming industry standards. Overcoming wellbore drilling instability in shale formations will always present one of the major challenges to our drilling engineers. What if this shale rock is also fractured? What would be the necessary theories and tools to apply in Real-Time to model these types of problems? What should be the drilling fluid chemistry and salt concentrations if the drilling fluid is water based mud?

The answer to these challenging problems lies in the theory behind the models used in the industry. Poromechanics, or the poroelastic theory, as it is more commonly known, could couple the diffusion processes of the fluid mud pressure, chemistry, temperature, in-situ stresses and the fracture pressure with formation pressure disturbance, in the case of fractured shale formation. In this paper the poromechanics approach and the estimation of the mud weight stability for the vertical or the inclined wellbore are briefly discussed and presented. These solutions, implemented in the software RT-PBORE-3D, are capable of analyzing Real-Time Wellbore Stability in sound and/or fractured shale rock formations.

### Introduction

In wellbore drilling, the pore pressure differential between the drilling mud and the drilled formation is governed by the diffusion process which is a time-dependent phenomenon. In addition, the downhole temperature and the chemical reactivity (mud/shale) are also time-dependent variables. As such, tools for Real-Time Wellbore drilling simulation should take into account these physical time-dependent processes, which involve among others stress/fluid pressure and temperature, coupled with the real-time monitoring data obtained periodically from LWD and SWD. The newly developed Real-Time Poromechanics Wellbore Stability simulator, RT-PBORE-3D, with its solid mechanics and poromechanics models is capable of coupling the real-time downhole data with the real-time-dependent diffusive processes, while upgrading the time-dependent mud weight window through the multi-layer drilling operations. The associated theories and their

implementation in RT-PBORE-3D are here discussed and examples of real-time drilling scenarios are illustrated.

Biot's theory of poroelasticity<sup>1</sup> represents an accurate and proven prediction theory of coupled time-dependent phenomena induced by stress perturbations in the geomechanical domain. The importance of these coupled processes in field applications from wellbore stability problems and reservoir management to design and analysis of laboratory rock testing procedures has already been well recognized. The extension of Biot's theory of Poromechanics to fractured rock formation within the framework of the dual-porosity approach has also been accomplished by Wilson and Aifantis<sup>2</sup>

RT-PBORE-3D is designed to simulate the three-dimensional time-dependent wellbore stability in real-time drilling operations for sound and fractured rock formations. The displayed values of mudweight windows for the corresponding drilled layers are calculated and updated as time and the drilling operation progress; thus illustrating the true nature of the phenomena of real-time diffusion, temperature gradient variations, and the evolution of chemical activities between the mud and the rock formation.

In this paper, a brief overview of both approaches to fractured and non-fractured rock formation is illustrated, and a validation of their use is also described. The applicability of RT-PBORE-3D is demonstrated through borehole stability analysis in multi-layer drilling operation with its associated time-dependent mudweight windows updates.

### Poromechanics Constitutive Relations

The time-dependent coupled diffusion-deformation effects including the temperature gradients and the chemical activity are best modeled within the general theory of poromechanics. The evolution in time of these dynamic and kinematic variables, within the consistent frame of the poroelastic theory, will allow real-time simulation.

The time-dependent coupling of solid matrix/grain deformation, pore fluid flow and the temperature gradient, for a sound rock formation, is governed by the following constitutive equations:

$$\sigma_{ij} = M_{ijkl} \varepsilon_{kl} - \alpha_{ij} p - \beta_{ij} T \dots\dots\dots(1)$$

$$p = M(\zeta - \alpha_{ij} \varepsilon_{ij} + \beta_m T) \dots\dots\dots(2)$$

Eq. (1) describes how the overall strains of the porous rock rely on the applied total stresses, the pore pressure weighted by Biot's effective stress tensor  $\alpha_{ij}$ , and the temperature gradient weighted by the thermic coefficient  $\beta_{ij}$ . Eq. (2), on the other hand, indicates that the fluid pore pressure is not only related to the pore fluid content variation,  $\zeta$ , but is also affected by the deformation of the rock solid matrix and the change in temperature. It should be noted that under isothermal conditions, the terms  $\beta_{ij}T$  and  $\beta_m T$  do not contribute.

Fractured rock formation is modeled within the framework of dual-porosity. Specifically, two overlapping and separate continua are considered, one for matrix block and the other for fractures. Fig. 1 provides the dual-porosity realization of naturally fractured rock in this sense. With the introduction of the fractured medium, both the stresses and pore pressures are modified due to the additional coupling of deformation, fluid flow and temperature gradient in the fracture. The constitutive equations for a fractured rock are given as:

$$\sigma_{ij} = M_{ijkl}^{I,II} \left( \varepsilon_{kl} - C_{klmn}^I \alpha_{mn}^I P^I - C_{klmn}^{II} \alpha_{mn}^{II} P^{II} \right) - (C_{klmn}^I \beta_{mn}^I + C_{klmn}^{II} \beta_{mn}^{II}) T \dots\dots\dots(3)$$

$$P^I = M^I (\zeta^I - M_{ijkl}^{I,II} C_{klmn}^I \alpha_{mn}^I \varepsilon_{ij} + \beta_m^I T) \dots\dots\dots(4)$$

$$P^{II} = M^{II} (\zeta^{II} - M_{ijkl}^{I,II} C_{klmn}^{II} \alpha_{mn}^{II} \varepsilon_{ij} + \beta_m^{II} T) \dots\dots\dots(5)$$

In the above equations, the superscripts I and II refer to the rock matrix and the fracture medium respectively,  $M_{ijkl}^{I,II}$  is the drained elastic modulus tensor for the whole solid domain,  $C_{klmn}^I$  and  $C_{klmn}^{II}$  are the compliance tensor for the corresponding media. Eq. (3) to (5) are direct extension of Eq. (1) and (2) in the approach to naturally fractured rocks using dual porosity concept. In writing Eq. (3), it is assumed that the changes in applied total stresses in each medium are equal and the overall deformations are obtained by adding the strains of the two media. Therefore, the overall strains of the fractured rock are governed by the applied total stress, the fluid pore pressure in each medium and the temperature gradient. The fluid pore pressures response equations are analogous to that of Eq. (2) except that the strain in each is expressed as a portion of the overall deformation.

In the following sections "we" will illustrate the implementation and the benefits, of these constitutive relations and their associate field equations, in the

solution of the aforementioned problems related to industry field applications.

### RT-PBORE-3D: Poromechanics Approach to Real-Time Wellbore Stability Applications

Real-time wellbore stability analysis is only possible if the time-dependent processes that are responsible for instability and failures during wellbore drilling are updated periodically from the real-time data collected from the various tools in MWD. Time-dependency in real-time wellbore stability applications has two folds: (1) allows updating of in-situ stresses, pore pressure and rock and drilling mud properties as the drill bit moves ahead; and (2) takes into account the time-dependent coupled phenomena of pore fluid diffusion, temperature gradient and formation stress variation. These coupled diffusion-deformation processes, in wellbore drilling mechanics, are naturally accounted for in the aforementioned constitutive modeling using the theory of poroelasticity<sup>1</sup>.

Analytical solutions for inclined boreholes in a general three-dimensional in-situ state of stress, accounting for time-dependent fluid diffusion, thermal and chemical effects, and rock formation material anisotropy, have been published and extensively applied in evaluating potential time-dependent effects on wellbore stability.<sup>3-8</sup> These solutions are implemented in the software, RT-PBORE-3D, developed for real-time drilling application. The solutions can perform analyses of stress/pore-pressure, formation failure, mudweight and mud salinity, temperature effect, etc. design for drilling in shale formations.

RT-PBORE-3D is equipped with a state-of-the-art user-friendly interface to facilitate data input and presentation of the output results. The software allows the real-time updating data from MWD tools and implementation in the time evolution design of wellbore-drilling program for mud-weight pressure windows, mud salinity, and wellbore depth-gradient analysis. These capabilities allow drilling engineers to make the necessary "on-rig" decisions on well control and potential critical time effects in drilling as well as completions, (e.g., time of casing placement and/or cementing, potential blow ups, etc.).

### Wellbore Stability Analysis using RT-PBORE-3D

In this section, the use of RT-PBORE-3D is demonstrated in several field examples. The inclined wellbore problem which represents a general class of three-dimension wellbore geometry from vertical to horizontal wells is used hereafter. The Figures 1, 2 and 3 illustrate the corresponding geometries of the problem in both single-porosity and naturally fractured dual-porosity rock formations. Fig. 4 shows a sample input data screen from RT-PBORE-3D. Relevant data such as wellbore orientation, in-situ stress and pore pressure gradients, material properties i.e., the elastic modulus,

Poisson's ratio etc., rock failure parameters and the particular model to be used in the analysis are imported from Excel sheets and/or ASCII files, consistent with outputs from MWD, SWD, PWD, etc. A sample Excel sheet used in RT-PBORE-3D is shown in Fig. 5. To date PBORE-3D<sup>9</sup> (earlier versions of RT-PBORE-3D) has been extensively used in the industry in field operations under a variety of scenarios.<sup>6,8</sup>

The real-time analysis module in RT-PBORE-3D was applied to a pilot well drilled in the North Sea. The input parameters used for development of the borehole stability model are as given in Table 1. In this case an elastic analysis was carried out for both, the sandstone and mudstone layers encountered and the collapse, fracturing and the stability mudweights were computed as shown in Fig. 6. Additionally, a similar analysis was carried out for a horizontal well drilled in the same field as the pilot well. Table 2 summarizes the mudweights predicted by RT-PBORE-3D and those used in the field.<sup>10</sup>

A poroelastic analysis of under-balanced drilling was carried out for a horizontal well in a highly depleted reservoir in Lake Maracaibo, Venezuela. The input parameters used are as given in Table 3. The collapse, fracturing and the stability mudweights for a given time are as shown in Fig. 7. RT-PBORE-3D predicted a safe mudweight of 2.7 ppg to be used throughout the drilling operation which compares favorably with the actual mudweight of 2.5 ppg used in the field.<sup>11</sup>

RT-PBORE-3D is now designed to accommodate real-time input data from generic Excel<sup>TM</sup> sheets that contain only relevant data at required depths. The user is provided the freedom to pick the analysis type (elastic or poroelastic), isotropy type (isotropic or transversely isotropic), pore pressure boundary conditions (permeable or impermeable) and the shear failure criteria (see Fig. 8). The data is imported periodically from standard Excel<sup>TM</sup> files that are organized in a specific format and the mudweight window for each layer is reupdated accordingly. Fig. 9 shows the results for an isotropic, poroelastic, permeable mudweight analysis for 3 depths using the Mohr-Coulomb criteria. RT-PBORE-3D also suggests the use of appropriate casing when the mudweight for collapse exceeds that for fracturing. Results are presented at a fractional distance into the formation, thus assuming strain relaxation on the immediate wellbore wall. Fig. 10 shows a snapshot of the data used, when viewed from within RT-PBORE-3D.

Analytical solutions for fractured formations based on the dual-porosity approach i.e., Eq. (3) to (5) has been developed and are incorporated into RT-PBORE-3D. In Figure 11 the mudweight window for instantaneous drilling of a permeable inclined borehole in a fractured rock formation is shown. For comparison purpose, the mudweight window for the corresponding single-porosity (non-fractured) rock is also plotted. Table 4 provides the data set used to generate the plot. It is obvious that the

dual-porosity behavior of the fractured system deviate from the single-porosity as the mudweight window is shifted upward. Thus, the effect of fractures in a fractured rock can not be overlooked.

## Conclusions

The study showed that time-dependency in wellbore stability can be critically examined for real-time support via a poromechanics approach.

Solutions for an inclined wellbore drilled in fractured or intact formations under a three-dimensional in-situ state of stress have been developed as part of the present research. These solutions are based on the poromechanics models, along with its conventional solid mechanics counterpart models. The solutions are all in analytical forms making RT-PBORE-3D efficient software for practicing engineers to simulate "real-time" analyses.

## Acknowledgements

This research work is supported by funds from the Rock Mechanics Consortium at the University of Oklahoma.

## Nomenclature

$\varphi_x$  = azimuth angle of the bore hole

$\varphi_y$  = inclination angle of the bore hole

LWD = logging while drilling

$M$  = Biot's modulus

$M_{ijkl}$  = elastic modulus tensor

MWD = measurement while drilling

ppg = pound per gallon

ROP = drilling rate of penetration

rpm = revolutions per minute

$S_H$  = maximum horizontal insitu principal stress gradient

$S_h$  = minimum horizontal insitu principal stress gradient

$S_v$  = vertical insitu principal stress gradient

$S_x, S_y, S_z, S_{xy}, S_{yz}, S_{xz}$  = local borehole stress insitu stress

$p_o$  = virgin pore pressure gradient

TD = total depth

TVD = true vertical depth

## References

1. Biot, M.A.: "General Theory of Three-Dimensional Consolidation." *Journal of Applied Physics*, V.12, pp.155-164, 1941.
2. Wilson, R.K. and Aifantis E.C.: "On the Theory of Consolidation with Double Porosity," *International Journal of Engineering Science*, Vol. 20, pp. 1009-1035, 1982.
3. Cui, L., Cheng, A. H-D., and Abousleiman, Y.: "Poroelastic solution of an inclined borehole," *ASME J. Appl. Mech.*, (1997), **64**, pp 32-37.
4. Abousleiman, Y. and Cui, L.: "Poroelastic Solutions in Transversely Isotropic Media for Wellbore and Cylinders," *International Journal of Solids Structures*, V.35, pp. 4905-4927, 1998.

5. Abousleiman, Y. and Ekbote, S.: "Porothermoelasticity in Transversely Isotropic Porous Materials," *under review, Journal of Applied Mechanics, ASME*.
6. Abousleiman, Y. *et al.*: "Time-dependent wellbore (in)stability predictions: Theory and Case Study", paper SPE 62796 presented at the 2000 IADC/SPE Asia Pacific Drilling Technology held in Kuala Lumpur, Malaysia 11–13 September 2000.
7. Ekbote, S.: "Poromechanics Wellbore Stability: Theory and Applications", Ph.D. Dissertation, the University of Oklahoma, 2002.
8. Abousleiman, Y. *et al.*: "Time-dependent wellbore-stability predictions", *J. of Petroleum Technology, JPT, Drilling Technology*, February, 2001.
9. Abousleiman, Y. *et al.*: "Tools in Poromechanics with Laboratory and Field Applications", *Proceedings of 2<sup>nd</sup> Biot Conference on Poromechanics*, France, Grenoble, 2002.
10. Collins, P.M.: "Geomechanics and wellbore stability design of an offshore horizontal well, North Sea", SPE 78975 presented at the 2002 SPE International Thermal Operations and Heavy Oil Symposium and International Horizontal Well Technology Conference held in Calgary, Alberta, Canada 4-7 November, 2002.
11. Parra, J.G., Gennaro and D.De: "Wellbore stability simulations for underbalanced drilling operations in highly depleted reservoirs", SPE 65512 presented at the 2000 SPE/Petroleum Society of CIM International Conference on Horizontal Well Technology held in Calgary, Alberta, Canada, 6-8 November, 2000.

## Tables

Table 1. Input parameters for real-time wellbore stability analysis (North Sea)

| Parameter                                  | Value       | Value       |
|--|-------------|-------------|
| Depth Range (ft)                           | 8,776-9,000 | 9,000-9,500 |
| Rock Type                                  | Sandstone   | Mudstone    |
| Overburden Stress Gradient, $S_v$ (psi/ft) | 1.0         | 1.0         |
| Maximum Horizontal Stress, $S_H$ (psi/ft)  | 0.75        | 0.75        |
| Minimum Horizontal Stress, $S_h$ (psi/ft)  | 0.61        | 0.61        |
| Pore Pressure, $P_o$ (psi/ft)              | 0.48        | 0.48        |
| Cohesion (psi)                             | 1,252.3     | 721         |
| Friction Angle (degrees)                   | 38.7        | 52.9        |
| Young's Elastic Modulus (psi)              | 2,250,000   | 4,000,000   |
| Poisson's Ratio                            | 0.16        | 0.33        |

Table 2. Comparison of mudweights predicted by RT-PBORE-3D with actual mudweights used

| Well              | Mudweights (lb/gal) |        |
|-------------------|---------------------|--------|
|                   | RT-PBORE-3D         | Actual |
| P2-NE2-Pilot      | 10.8                | 10.43  |
| P2-NE2-Horizontal | 10.8                | 10.43  |

Table 3. Input parameters for poroelastic analysis of under-balanced drilling (Lake Maracaibo, Venezuela)

| Parameter                           | Value          |
|-------------------------------------|----------------|
| Hole Angle (degrees)                | 90             |
| Azimuth (degrees)                   | 0              |
| $S_v/S_H/S_n$ gradients (psi/ft)    | 0.95/0.64/0.52 |
| Pore pressure gradient (psi/ft)     | 0.14           |
| Cohesion (psi)                      | 2020           |
| Friction angle (degrees)            | 35.5           |
| Elastic Modulus (psi)               | 2400000        |
| Poisson's ratio                     | 0.18           |
| Biot's Effective Stress Coefficient | 0.91           |
| Undrained Poisson's ratio           | 0.43           |
| Permeability (md)                   | 100            |
| Fluid viscosity (poise)             | 0.07           |

Table 4. Input parameters for dual-porosity mudweight analysis of the inclined wellbore in fractured formation

| Parameters                      | Single Porosity     | Double Porosity |
|---------------------------------|---------------------|-----------------|
| $S_v/S_H/S_n/P_o$ (psi/ft)      | 1.11/1.28/0.88/0.43 |                 |
| Azimuth (degrees)               | 70                  |                 |
| Matrix Permeability (md)        | 0.001               | 0.001           |
| Fracture Permeability (md)      |                     | 0.1             |
| Matrix Porosity (fraction)      | 0.02                | 0.02            |
| Fracture Porosity (fraction)    |                     | 0.002           |
| Modulus Young (psi)             | 268,755             | 268,755         |
| Poisson Ratio (dimensionless)   | 0.219               | 0.219           |
| Bulk Grain Modulus (psi)        | 4,986,397           | 4,986,397       |
| Fracture Normal Stiffness (psi) |                     | 498,639         |
| Fracture Spacing (ft)           |                     | 1.64            |
| Bulk Fluid Modulus (psi)        | 35,244              | 35,244          |
| Fluid Viscosity (cp)            | 1                   | 1               |
| Time (day)                      | 0.001               | 0.001           |

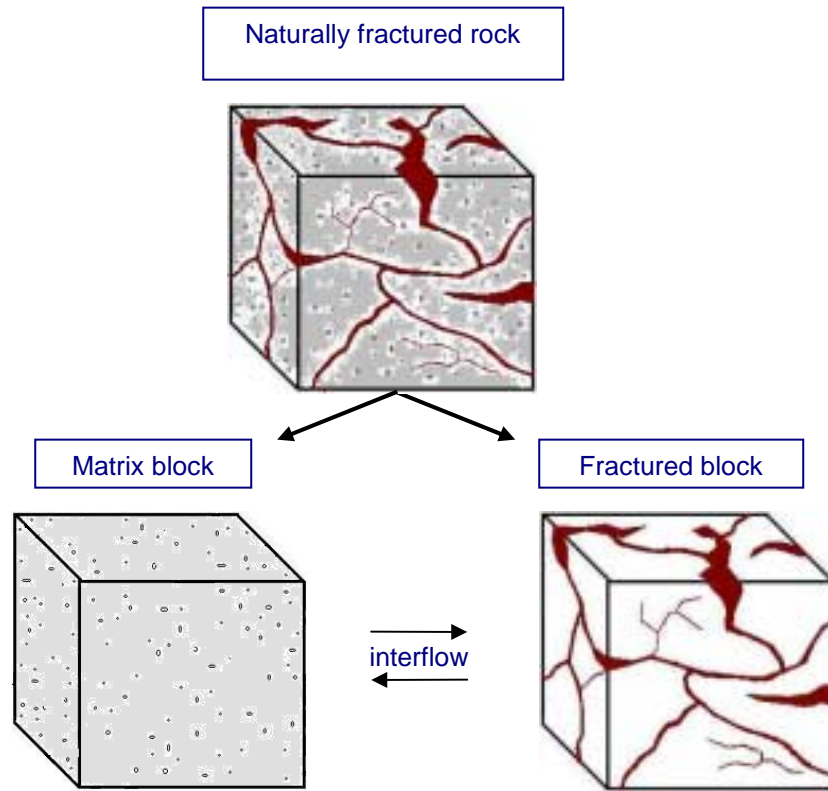


Figure 1: Visualization of a double porosity naturally fractured rock formation

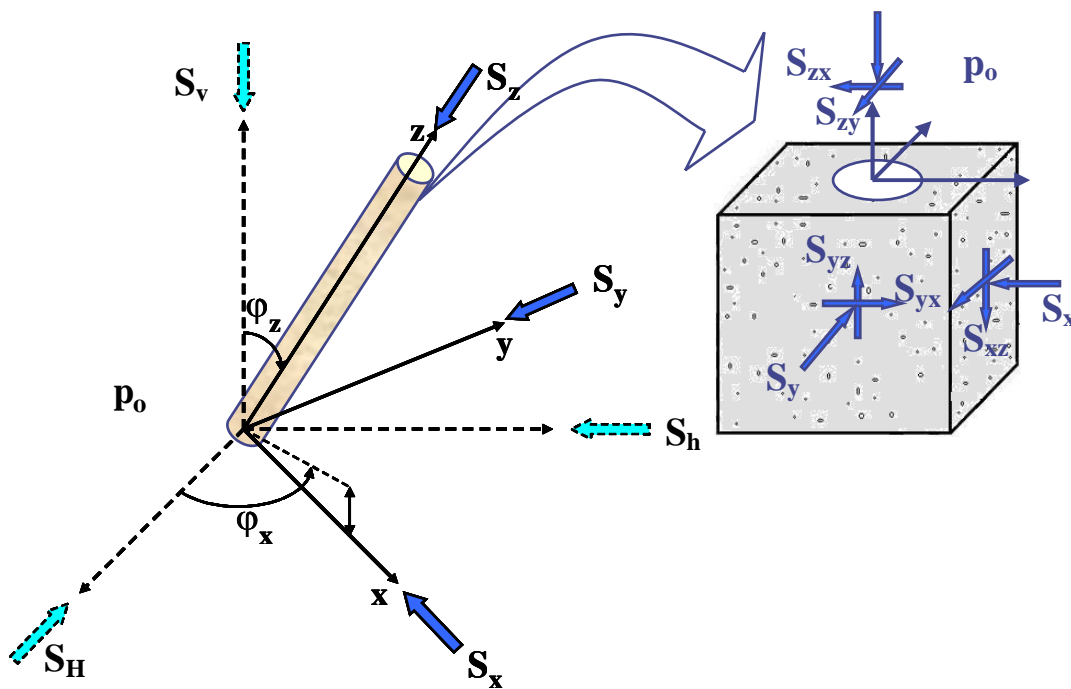


Figure 2: Geometry of the inclined wellbore problem in single-porosity rock

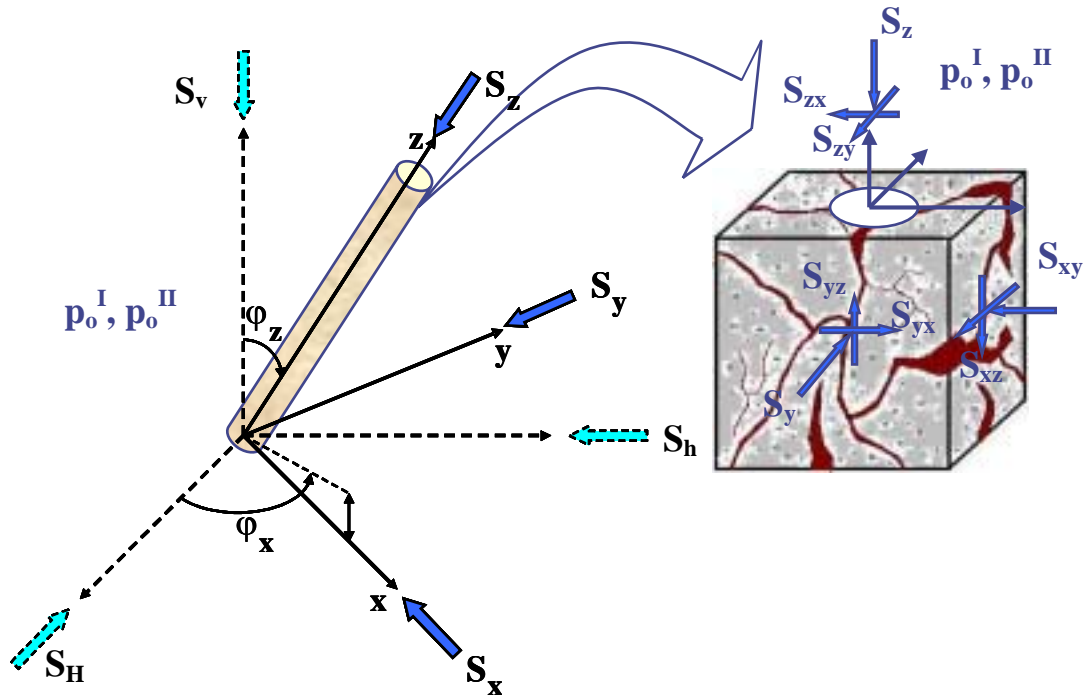


Figure 3: Geometry of the inclined wellbore problem in dual-porosity fractured rock

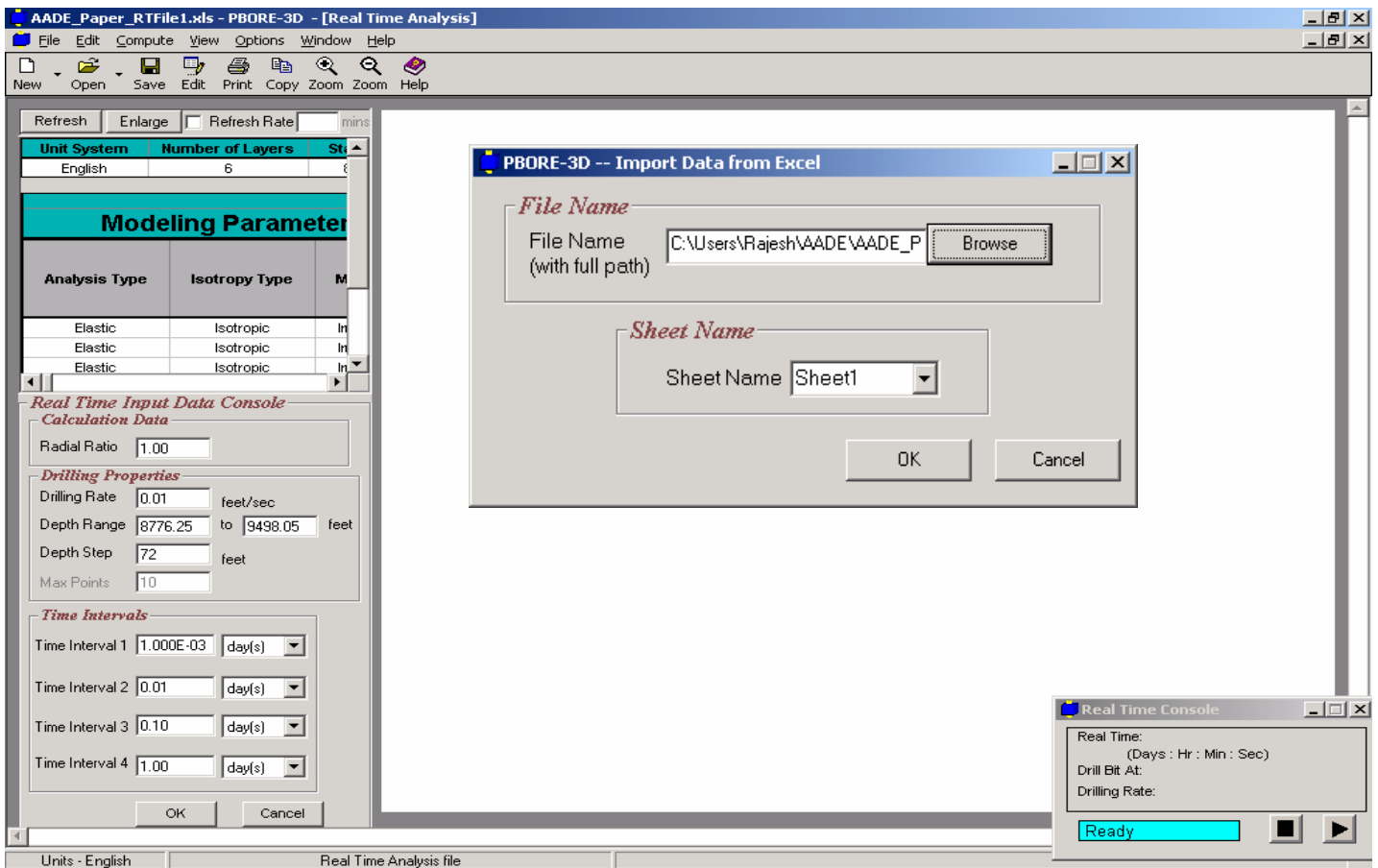


Figure 4: The RT-PBORE-3D Input data screen

|    | A                          | B                       | C                  | D                        | E                    | F                  | G           | H                  | I            | J                    | K                        |
|----|----------------------------|-------------------------|--------------------|--------------------------|----------------------|--------------------|-------------|--------------------|--------------|----------------------|--------------------------|
| 1  | <b>Unit System</b>         | <b>Number of Layers</b> | <b>Start Depth</b> | <b>Hole Radius</b>       | <b>Drilling Rate</b> | <b>Time Int. 1</b> | <b>Unit</b> | <b>Time Int. 2</b> | <b>Unit</b>  | <b>Time Int. 3</b>   | <b>Unit</b>              |
| 2  | English                    | 6                       | 8776.25            | 0.33                     | 1.00E-02             | 1.00E-03           | days        | 1.00E-02           | days         | 1.00E-01             | days                     |
| 3  |                            |                         |                    |                          |                      |                    |             |                    |              |                      |                          |
| 4  | <b>Modeling Parameters</b> |                         |                    | <b>Wellbore Geometry</b> |                      |                    |             |                    |              |                      |                          |
| 5  | <b>Modeling Parameters</b> |                         |                    | <b>Wellbore Geometry</b> |                      |                    |             |                    |              |                      |                          |
| 6  | <b>Analysis Type</b>       | <b>Isotropy Type</b>    | <b>Model Type</b>  | <b>Thickness</b>         | <b>Hole Angle</b>    | <b>Azimuth</b>     | <b>Sv</b>   | <b>SHMax</b>       | <b>SHMin</b> | <b>Pore Pressure</b> | <b>Failure Criterion</b> |
| 7  | Elastic                    | Isotropic               | Impermable         | 65.62                    | 55                   | 90                 | 1           | 0.75               | 0.61         | 0.48                 | Drucker-F                |
| 8  | Elastic                    | Isotropic               | Impermable         | 98.43                    | 55                   | 90                 | 1           | 0.75               | 0.61         | 0.48                 | Drucker-F                |
| 9  | Elastic                    | Isotropic               | Impermable         | 65.62                    | 55                   | 90                 | 1           | 0.75               | 0.61         | 0.48                 | Drucker-F                |
| 10 | Elastic                    | Isotropic               | Impermable         | 229.66                   | 55                   | 90                 | 1           | 0.75               | 0.61         | 0.48                 | Drucker-F                |
| 11 | Elastic                    | Isotropic               | Impermable         | 32.81                    | 55                   | 90                 | 1           | 0.75               | 0.61         | 0.48                 | Drucker-F                |
| 12 | Elastic                    | Isotropic               | Impermable         | 229.66                   | 55                   | 90                 | 1           | 0.75               | 0.61         | 0.48                 | Drucker-F                |
| 13 |                            |                         |                    |                          |                      |                    |             |                    |              |                      |                          |
| 14 |                            |                         |                    |                          |                      |                    |             |                    |              |                      |                          |
| 15 |                            |                         |                    |                          |                      |                    |             |                    |              |                      |                          |
| 16 |                            |                         |                    |                          |                      |                    |             |                    |              |                      |                          |
| 17 |                            |                         |                    |                          |                      |                    |             |                    |              |                      |                          |
| 18 |                            |                         |                    |                          |                      |                    |             |                    |              |                      |                          |
| 19 |                            |                         |                    |                          |                      |                    |             |                    |              |                      |                          |
| 20 |                            |                         |                    |                          |                      |                    |             |                    |              |                      |                          |
| 21 |                            |                         |                    |                          |                      |                    |             |                    |              |                      |                          |
| 22 |                            |                         |                    |                          |                      |                    |             |                    |              |                      |                          |
| 23 |                            |                         |                    |                          |                      |                    |             |                    |              |                      |                          |
| 24 |                            |                         |                    |                          |                      |                    |             |                    |              |                      |                          |
| 25 |                            |                         |                    |                          |                      |                    |             |                    |              |                      |                          |

Figure 5: A view of the Excel input data sheet for Real-Time Analysis

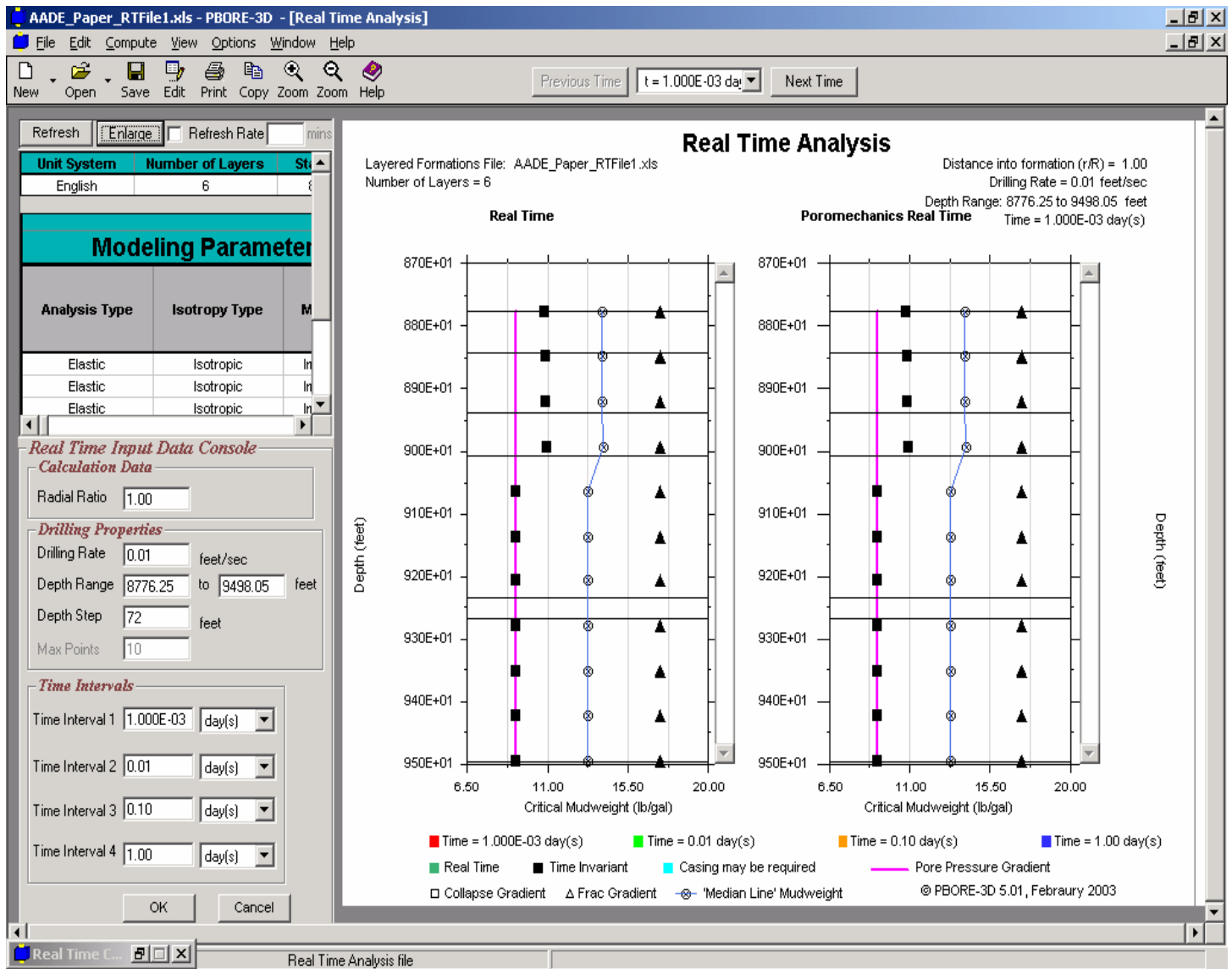


Figure 6: Collapse, fracturing and median-Line mudweights from real-time analysis (North Sea)

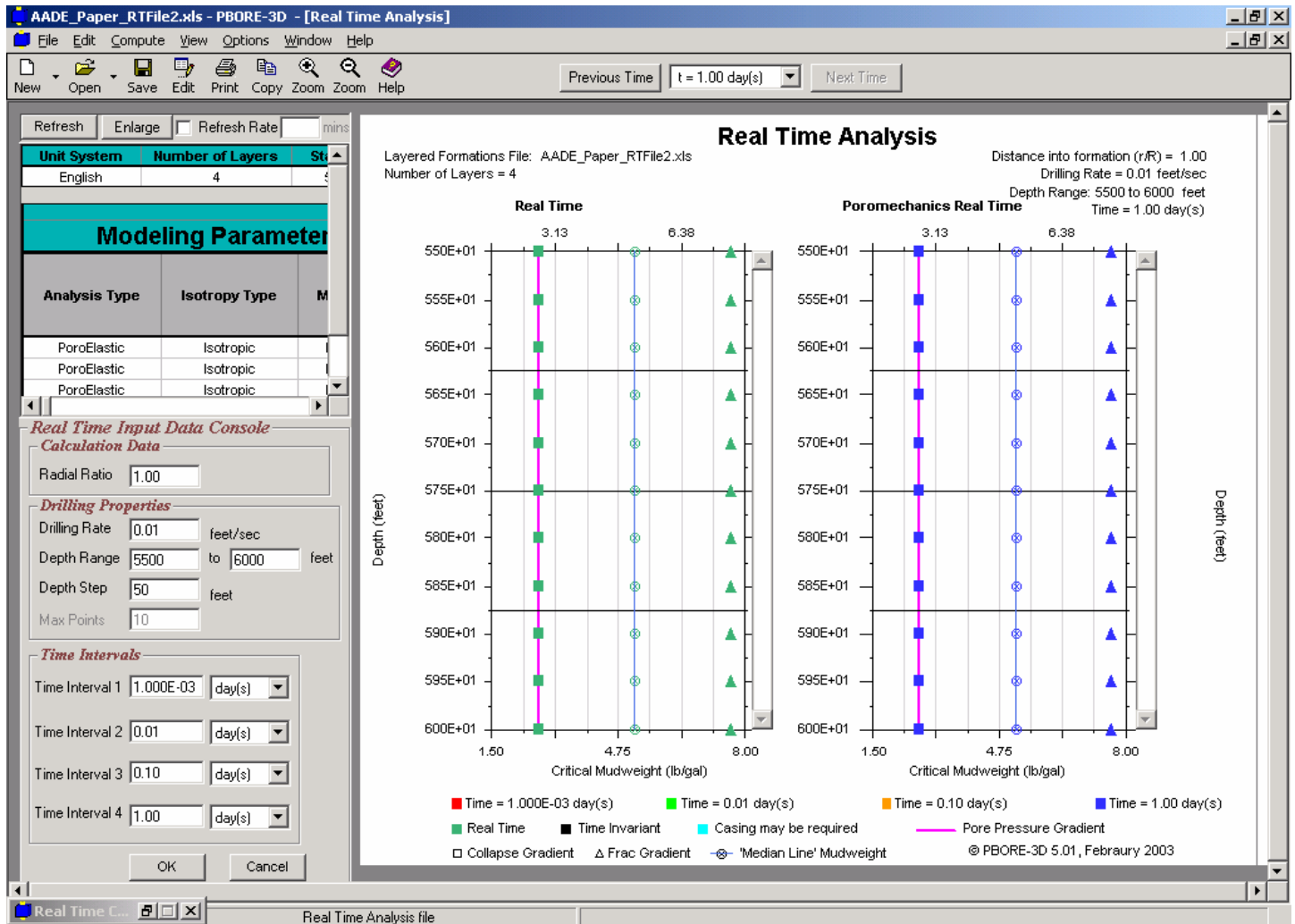


Figure 7: Collapse, fracturing and median-Line mudweights from real-time analysis (Lake Maracaibo, Venezuela)

**Generic Excel Input**

*Isotropy Type*

- Isotropic
- Transversely Isotropic

*Model Type*

- Permeable
- Impermeable

Borehole Radius  m

*File Name*

File Name (with full path)

*Sheet Name*

Sheet Name

*Shear Failure Parameters*

- Mohr - Coulomb (MCFC)
- Drucker - Prager (DPFC)
- Modified Lade Criterion (MLFC)

*Unit System*

- English
- International

*Analysis Type*

*Conventional Elastic Approach*

- Elastic
- Thermoelastic
- Viscoelastic
- Chemoelastic
- Chemothermoelastic

*Poromechanics Approach*

- Poroelastic
- Porothermoelastic
- Poroviscoelastic
- Porochemoelastic
- Porochemothermoelastic

Figure 8: Input screen for the generic Excel file option in RT-PBORE-3D

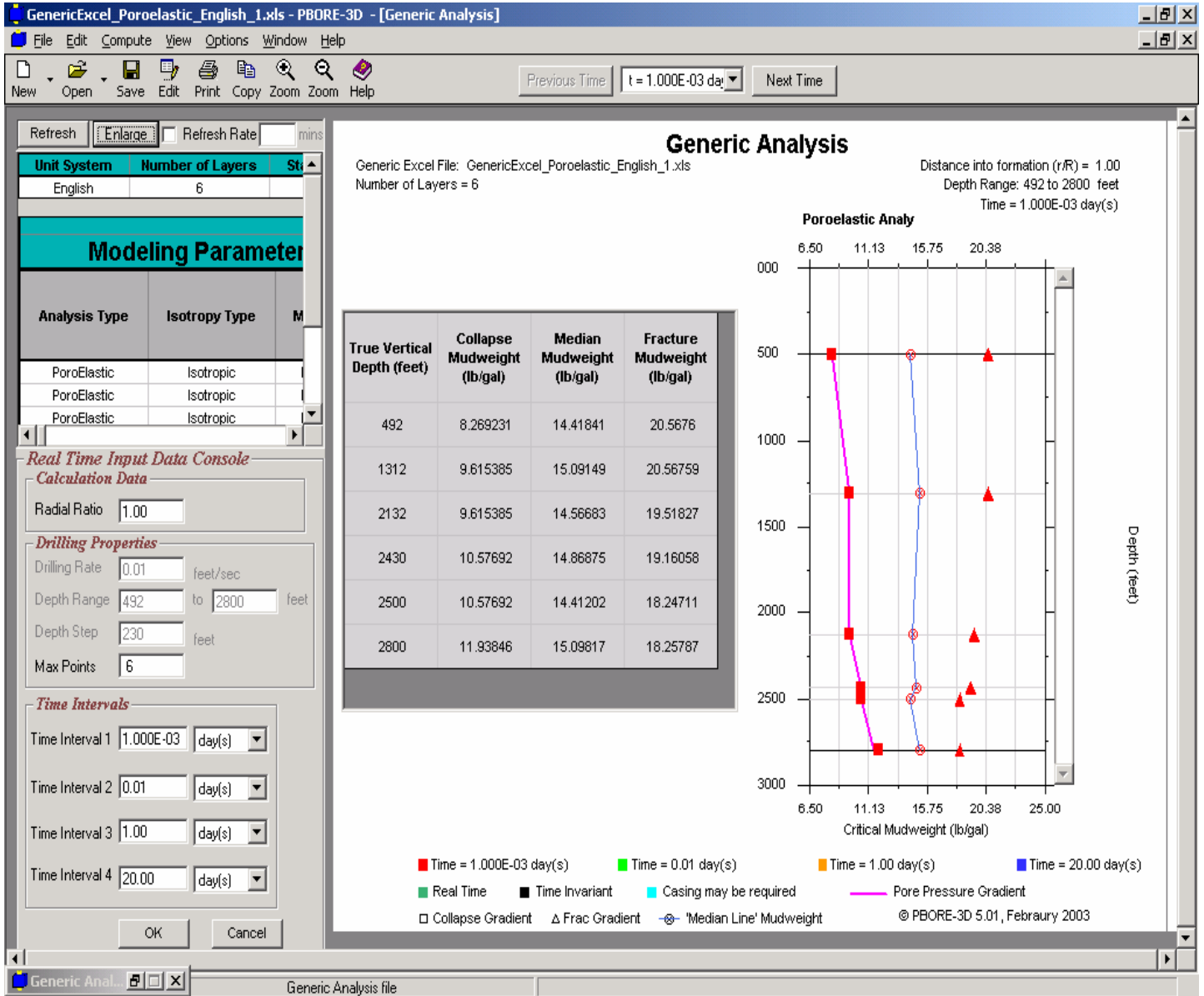


Figure 9: Results from the Generic Excel File option using a permeable, poroelastic analysis with the Mohr-Coulomb failure criteria.

| PBORE3D - View Input in Grid |                  |             |                     |                 |             |             |             |   |
|------------------------------|------------------|-------------|---------------------|-----------------|-------------|-------------|-------------|---|
| Unit System                  | Number of Layers | Start Depth | Hole Radius         | Drilling Rate   | Time Int. 1 | Unit        | Time Int. 2 | U |
| English                      | 6                | 492.00      | 0.10                | 0.01            | 1.000E-03   | days        | 0.01        | 0 |
| Modeling Parameters          |                  |             |                     | Wellbore Geomet |             |             |             |   |
| Analysis Type                | Isotropy Type    | Model Type  | True Vertical Depth | Hole Angle      | Azimuth     | Sv Gradient | SHMax Grad  |   |
| PoroElastic                  | Isotropic        | Permeable   | 492.00              | 50.00           | 30.00       | 1.28        | 1.11        |   |
| PoroElastic                  | Isotropic        | Permeable   | 1312.00             | 55.00           | 30.00       | 1.28        | 1.11        |   |
| PoroElastic                  | Isotropic        | Permeable   | 2132.00             | 60.00           | 30.00       | 1.28        | 1.11        |   |
| PoroElastic                  | Isotropic        | Permeable   | 2430.00             | 65.00           | 30.00       | 1.28        | 1.11        |   |
| PoroElastic                  | Isotropic        | Permeable   | 2500.00             | 65.00           | 30.00       | 1.28        | 1.11        |   |
| PoroElastic                  | Isotropic        | Permeable   | 2800.00             | 65.00           | 30.00       | 1.28        | 1.11        |   |

Figure 10: Snapshot of data used to generate results in Figure 9 (when viewed from within RT-PBORE-3D).

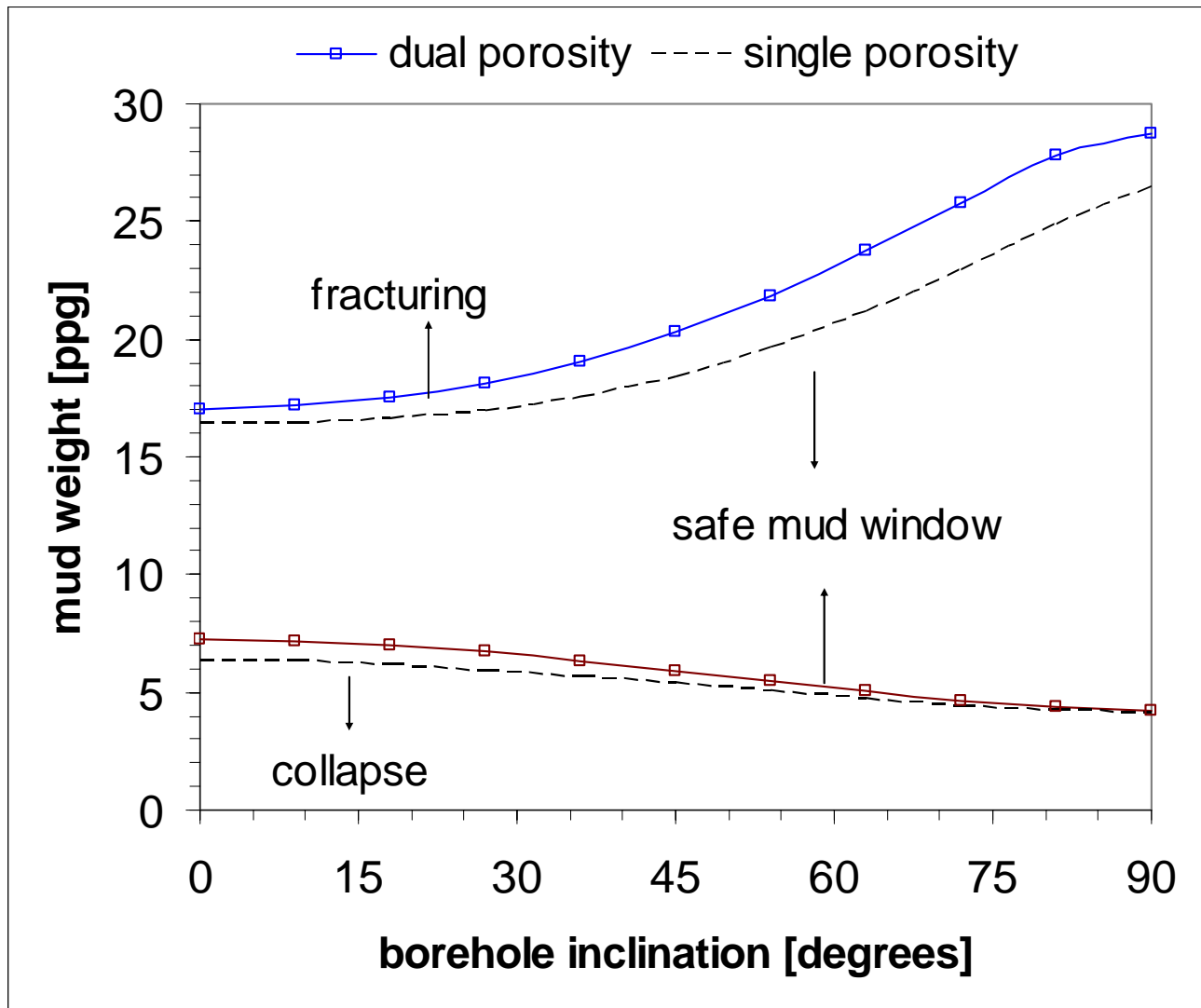


Figure 11: Mudweight window for an inclined wellbore in naturally fractured rock formation after 0.001 day